JOURNAL OF SYNCHROTRON RADIATION

ISSN 1600-5775

Investigation of third-order nonlinear dynamical X-ray diffraction based on a new exact solution

Minas K. Balyan*

Faculty of Physics, Yerevan State University, Alex Manoogian 1, Yerevan 0025, Armenia.
*Correspondence e-mail: mbalyan@ysu.am

Received 13 February 2020
Accepted 19 May 2020

Edited by A. Momose, Tohoku University, Japan

Keywords: nonlinear dynamical diffraction; X-ray; crystal; third-order nonlinearity; exact solution..

Third-order nonlinear two-wave dynamical X-ray diffraction in a crystal is considered. For the Laue symmetrical case of diffraction a new exact solution is obtained. The solution is presented via Jacobi elliptic functions. Two input free parameters are essential: the deviation parameter from the Bragg exact angle and the intensity of the incident wave. It is shown that the behavior of the field inside the crystal is determined by the sign of a certain combination of these parameters. For negative and positive signs of this combination, the wavefield is periodic and the nonlinear Pendellösung effect takes place. For the nonlinear Pendellösung distance the appropriate expressions are obtained. When the above-mentioned combination is zero, the behavior of the field can be periodic as well as non-periodic and the solution is presented by elementary functions. In the nonperiodic case, the nonlinear case Pendellösung distance tends to infinity. The wavefield diffracts and propagates in a medium, whose susceptibility is modulated by the amplitudes of the wavefields. The behavior of the wavefield can be described also by an effective deviation from the Bragg exact angle. This deviation is also a function of the wavefields.

1. Introduction

Theoretical and experimental investigations of nonlinear hard X-ray diffraction and other nonlinear effects of X-ray interactions with matter are motivated by the success of high-intensity hard X-ray synchrotron sources and X-ray free-electron lasers (XFELs).

Physically, how do nonlinear phenomena of X-ray interactions with matter occur? The basis of all the processes of interactions of X-ray radiation with matter is the interaction of the X-ray wave with the electrons of the medium. The force of an external electromagnetic field and the force associated with the intra-atomic potential act on each electron in the medium (Boyd, 2003). Thus each electron will experience the force $\mathbf{F}_{in} + e\mathbf{E} + e[\mathbf{vB}]$. Here the intra-atomic force $\mathbf{F}_{in} = -\nabla U_{in}$, where U_{in} is intra-atomic potential energy. When there is no external field, the electron is in its equilibrium position, where $\mathbf{F}_{in} = -\nabla U_{in} = 0$. The external electrical field strength in the nonlinear case is close to the intra-atomic electrical field; it may be one or two orders less, since the nonlinear effects accumulate during the propagation of the wave. Under the action of an external field, the intra-atomic restoring force arises. If we expand the atomic potential energy near the equilibrium point, then depending on the intensity of the external field we can restrict ourselves to a quadratic, cubic or fourth-degree term. Accordingly, the restoring force will be linear in coordinate, quadratic or cubic. If we neglect the Lorentz magnetic force, then solving the classical mechanical equation of motion, using the perturbation theory, we can find the electron coordinate up to third-order nonlinear terms on **E**

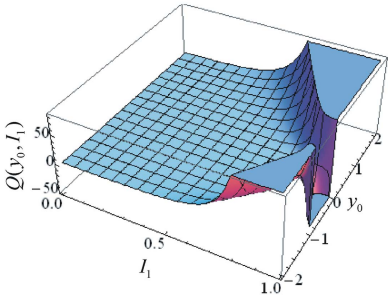

(Boyd, 2003). Thus the medium response will be described with up to third-order nonlinear polarization. When the frequency of the external field is sufficiently greater than the resonance frequencies of the electrons, then the restoring force can be omitted and there is no nonlinear term. This model is called the free electron model or cold collisionless plasma model. For this model the nonlinear terms can arise from the Lorentz magnetic force (Eisenberger & McCall, 1971). Thus there are two models of nonlinearity. The first takes into account the restoring nonlinear force, and the second takes into account the nonlinearities coming from the magnetic force. We can, therefore, distinguish the nonlinearities of bonding electrons, when the restoring force is taken into account, and the nonlinearities of free electrons, when the restoring force is omitted.

The quantum mechanical approach to the nonlinear polarization is based on the time-dependent perturbation theory of the Schrödinger equation. The motion of electrons without an external field is described by stationary states of the unperturbed Hamiltonian. The interaction with an external field generates some interaction terms in the Hamiltonian. Considering the interaction terms as perturbations, one can find the first-, second- and third-order corrections to the current density and wavefunctions and thus one can find the first-, second- and third-order corrections to the polarization (Boyd, 2003). The unperturbed wavefunctions of electrons are considered to be known.

The second- and the third-order polarizations can formally be written in the form $P^{(2)}(t) = \varepsilon_0 \chi^{(2)} E^2(t)$ and $P^{(3)}(t) = \varepsilon_0 \chi^{(3)} E^3(t)$ (Boyd, 2003), where χ is the nonlinear susceptibility and $\varepsilon_0 = 8.85 \times 10^{-12}$ F m^{-1} is the permittivity of free space. Assuming that the electrical field is the sum of two fields with frequencies ω_1 and ω_2, the following main second-order processes can be distinguished: $P^{(2)}(2\omega_1) \simeq E_1^2(\omega_1)$ or $P^{(2)}(2\omega_2) \simeq E_2^2(\omega_2)$ correspond to the second harmonic generation (SHG), $P^{(2)}(\omega_1 + \omega_2) \simeq E_1(\omega_1) E_2(\omega_2)$ corresponds to the sum frequency generation (SFG), $P^{(2)}(\omega_1 - \omega_2) \simeq E_1(\omega_1)\, E_2^*(\omega_2)$ is the difference frequency generation (DFG), $P^{(2)}(0 = \omega_1 - \omega_1 = \omega_2 - \omega_2) \simeq [E_1(\omega_1) E_1^*(\omega_1) + E_2(\omega_2) E_2^*(\omega_2)]$ is the optical rectification (OR).

One of the second-order nonlinear processes is the spontaneous parametric down conversion (PDC), when a field (photon), *i.e.* the pump, with a frequency ω_p, in a medium with a second-order nonlinear response, decays into two photons with frequencies ω_s and ω_i, so that $\omega_p = \omega_s + \omega_i$. These photons are called signal and idler photons. The corresponding polarizations are $P^{(2)}(\omega_s) \simeq E_p(\omega_p)\, E_i^*(\omega_i)$ and $P^{(2)}(\omega_i) \simeq E_p(\omega_p)\, E_s^*(\omega_s)$. In the X-ray region, PDC has been theoretically predicted in crystals (Freund & Levine, 1969). One of the photons, *e.g.* the signal, must have a frequency in the X-ray region. In the X-ray region the physical mechanism is the following: quantum noise at the signal and idler frequencies in the nonlinear crystal produce a fluctuating sum frequency polarization $P_p^{(2)}(\omega_p = \omega_s + \omega_i) \simeq E_s(\omega_s) E_i(\omega_i)$, which interacts with the external pump field (Freund, 1972). Besides the energy conservation, these three photons must also satisfy the momentum conservation law $k_p = k_s + k_i$. But for X-rays the refractive index is close to unity, and this conservation law cannot be satisfied in an amorphous medium due to the dispersion of the refractive index (Adams *et al.*, 2000). Meanwhile, in the crystals the conservation law can be written in the form $\mathbf{k}_p + \mathbf{h} = \mathbf{k}_s + \mathbf{k}_i$, where $\mathbf{h}$ is a reciprocal lattice vector (Freund & Levine, 1969). By choosing an appropriate reciprocal lattice vector the momentum conservation law can be satisfied in crystals. Three types of X-ray PDC are distinguished: (i) both signal and idler have X-ray region frequencies (XPDC); (ii) the signal frequency is in the X-ray region and the idler frequency lies in the optical range; and (iii) the signal frequency lies in the X-ray region and the idler frequency lies in the ultraviolet range (XUV) (Freund, 1972). In the last mentioned work it was predicted that for the first case the nonlinear interaction is governed by the total electron charge density, the second type of conversion is determined by the redistribution of the electron charge density, and the third type is determined by the charge distribution of valence electrons. Thus the experimental observation of PDC can be used for determination of electron charge density in materials. Another application would be quantum optics (Adams *et al.*, 2000). Observation of PDC of the first type has been reported by Eisenberger & McCall (1971). In theoretical work, Freund & Levine (1969) have shown that XPDC can be realized using 10 kW sources. Eisenberger & McCall (1971) used a 2 kW X-ray tube and Mo K_α radiation. The pump photon has energy 17 keV. Signal and idler photons with energies of 8.5 keV have been registered as a result of diffraction using a Be crystal. The binding energy of Be is 100 eV and the photon frequency is very large in comparison with resonance frequencies. So the free electron model is used. Relatively recently, XPDC has been observed in the works of Yoda *et al.* (1998) and Adams *et al.* (2000). In these works XPDC is observed using Bragg diffraction in diamond crystals. Synchrotron sources of X-rays are used. Using a synchrotron source makes it possible to use beams with small angular divergence, which is necessary to detect pairs of photons scattered to small solid angles. The diamond crystals used have a high degree of perfection and do not absorb the emitted photons strongly. XPDC has also been observed in Laue geometry (Shwartz *et al.*, 2012).

PDC of the second type is theoretically considered by Freund & Levine (1970). The experimental observation of the second kind of PDC, *i.e.* the PDC of X-rays into the optical regime, has been reported by Schori *et al.* (2017) (in this work see also the references about X-ray and optical wave mixing SFG and DFG processes). The authors used an X-ray synchrotron source of radiation.

The observation of PDC in the XUV was first reported in the work Danino & Freund (1981). In the experiment, 8 keV pump photons decay into signal photons with 7.7 keV energy and idler photons having an extreme ultraviolet (EUV) energy range of 335 eV. Bragg diffraction of the pump wave is performed using a LiF crystal. More recently, this effect has been studied, for example, by Tamasaku & Ishikawa (2007*a*,*b*). The first mentioned work is the first XUV experiment using X-ray synchrotron sources. The signal and idler waves propagate interacting with each other, but the back

influence of these waves on the intensity of the pump wave is neglected. The theory predicts a Lorentzian form of the rocking curve, but the experiment shows a peak followed by an unpredicted dip. The authors explain this dip as the result of interference between the Compton effect and XUV. In the second mentioned work the diffraction rocking curve dependence on the idler photon energy has been investigated. By decreasing the idler photon energy the rocking curves show a more pronounced dip. In the work of Tamasaku *et al.* (2009) using XUV in diamond, the second-order nonlinear susceptibility of diamond is measured. It was found that $|\chi^{(2)}_{220}| = 6 \times 10^{-17}$ esu $= 2.4 \times 10^{-20}$ m V^{-1} [according to Boyd (2003), $\chi^{(2)}$(MKS) $= 4.189 \times 10^{-4}\chi^{(2)}$ (Gaussian)]. In diamond and lithium fluoride crystals XUV is observed using a laboratory X-ray source (Borodin *et al.*, 2017). It is shown that the predictions of the free electron model (the nonlinearity arises from the magnetic force) agree with the experimental results in diamond. The Compton and Raman scattering form the noise. The Raman scattering is very weak far from the resonance. The XUV near the *K*-absorption edge of diamond and *L*-absorption edge of silicon were investigated by Barbiellini *et al.* (2015). Observation of collective nonlinear interactions in XUV processes has been reported by Borodin *et al.* (2019). An interpretation is proposed which includes nonlinear interactions with plasmons.

X-ray SHG, also being a second-order nonlinear effect, has been theoretically investigated by Nazarkin *et al.* (2003). In this work the effect is investigated using the free electron model. The term in the second-order nonlinear current density, which gives rise the SHG, is determined by the gradient of the charge density of free electrons. Thus the SHG of free electrons cannot be realized in homogeneous mediums. But X-ray SHG of free electrons can be realized in centrosymmetrical crystals. The phase matching condition is obeyed considering linear Bragg diffraction (both in Bragg and Laue geometries) of the formed second harmonic for an appropriate reciprocal lattice vector. The necessary intensity for observing X-ray SHG is estimated to start from 10^{16} W m^{-2}. The theory of SHG in XFELs has been discussed by Geloni *et al.* (2007). The observation of SHG in diamond has been reported by Shwartz *et al.* (2014). The used intensities exceed 10^{20} W m^{-2}. The SHG from focused ultrashort pulses is discussed in the work of Yudovich & Shwartz (2015).

X-ray and optical wave mixing, *i.e.* SFG, is experimentally investigated in the work of Glover *et al.* (2012). Discussions of DFG processes can be found in the works of Shwartz & Shwartz (2015), Minerbi & Shwartz (2019) and Cohen & Shwartz (2019).

It is interesting to note that the Compton effect and X-ray Raman scattering are second-order nonlinear processes (Bushuev & Kuz'min, 1977). X-ray Raman scattering is Compton scattering when the frequency of the photon is close to the resonance frequency of the electron. In this case the photon is scattered on a bound electron and the scattered photon frequency is shifted by the resonance frequency of the scattering electron. These inelastic processes make it possible to investigate the momentum–energy characteristics of mediums. Compton scattering allows the re-estimation of the linear susceptibility (Kolpakov *et al.*, 1978). Anomalous Compton scattering (nonlinear Compton effect) for a high-intensity incident X-ray beam has been observed by Fuchs *et al.* (2015). In nonlinear Compton scattering, three photons participate. The nonlinearity is related to relativistic effects of the electrons. The nonlinear response of an atom to intense ultrashort X-ray pulses is investigated experimentally by Doumy *et al.* (2011).

The formal representation of the third-order nonlinear polarization is $P^{(3)}(t) = \varepsilon_0\chi^{(3)}E^3(t)$ (Boyd, 2003). In the general case the wave can be a sum of fields with three different frequencies ω_1, ω_2 and ω_3. The resulting polarization contains 44 frequency components. Consider a simple case where the incident radiation has a frequency ω. The component of polarization $P^{(3)}(3\omega) = \varepsilon_0\chi^{(3)}E^3(\omega)$ corresponds to a nonlinear process called third-harmonic generation. Another important component of polarization is $P^{(3)}(\omega) = \varepsilon_0\chi^{(3)}E^2(\omega)E^*(\omega)$. This term introduces a contribution to susceptibility (refractive index) that depends on the intensity of radiation. A wave with the frequency of the incident wave propagates and diffracts in a medium with a self-induced refractive index. In optics, self-focusing phenomena connected with this term are known. For X-rays this term will describe the third-order nonlinear Bragg diffraction in crystals. Third-order nonlinear Bragg diffraction is very important since Bragg diffractive optical elements (monochromators, collimators, focusing elements) are commonly used for preparing beams with given parameters. The linear theory of Bragg diffraction works well for low intensities. Nowadays, for preparing high-intensity X-ray beams with given parameters, it is important to understand the properties of Bragg diffraction taking into account the third-order nonlinear term in the susceptibility. It is important to estimate the corresponding third-order nonlinear susceptibility for X-rays. Such an estimate will depend on the model of the scattering process. In Adams (2003), in the frame of time-dependent perturbation theory of the Schrödinger equation, the third-order contribution in the susceptibility of X-rays for low-Z materials ($Z < 10$) in the case of non-resonance electronic response is estimated to be $\chi^{(3)} \simeq 1.3 \times 10^{-32}$ esu $= 1.8 \times 10^{-40}$ m^2 V^{-2}, which is very small and can be neglected. That is why researchers concentrate on treating third-order nonlinear X-ray scattering using the free electron model (model of cold collisionless plasma), taking into account the nonlinearities coming from the magnetic force. Conti *et al.* (2008), using the third-order nonlinear cold plasma model, investigated the direct propagation of an intense X-ray beam. In the mentioned work for the third-order nonlinear susceptibility value the estimate $\chi^{(3)} \simeq 10^{-36}$ m^2 V^{-2} is obtained.

But the third-order nonlinearity can be investigated using another model. Let us consider the Ewald model of dipoles in crystals, well known in linear theory (James, 1950). This model works well in linear theory. The dipoles can be set in oscillation by radiation passing through the crystal. The classical equation of motion of a dipole in the linear approximation is $\mathbf{p} + \omega_0^2\mathbf{p} = e^2\mathbf{E}/m$. Let us extend this model of Ewald, and

quantum-mechanically consider the nonlinear dipole model (Balyan, 2015*a*). The interaction Hamiltonian of a dipole is $H' = -\mathbf{pE}$. For this model the third-order nonlinear term in the susceptibility was calculated by Boyd (2003) [formula (4.3.5)]. Using this result and considering the non-resonant case, when the external field frequency is higher than the resonance frequencies (such a case is usually realized for Bragg diffraction in such crystals as Si and Ge), in the work of Balyan (2015*a*) the following estimate is obtained for X-rays: $\chi^{(3)} \simeq 10^{-31}$–$10^{-33}$ m^2 V^{-2}. This estimate is essentially larger than the estimates obtained by Adams (2003) and Conti *et al.* (2008). The obtained value allows investigating Bragg diffraction taking into account the third-order nonlinear contribution. Iirrespective of the value of the third-order nonlinear susceptibility, the non-linear Bragg diffraction is of independent interest.

Third-order nonlinear X-ray four-wave mixing is investigated by Tanaka & Mukamel (2002), and X-ray two-photon absorption, also being a third-order nonlinear process, has been observed by Tamasaku *et al.* (2014).

Concluding this introduction, let us formulate the purpose of this work and its physical sense. As mentioned above, the third-order nonlinear interaction of X-rays with matter is determined by the fourth-rank susceptibility tensor $\chi^{(3)}(\omega_q; \omega_m, \omega_n, \omega_p, \mathbf{r})$ (Boyd, 2003), where the frequencies obey the relation $\omega_q = \omega_m + \omega_n + \omega_p$ and $\mathbf{r}$ is the radius vector of the observation point. If the incident wave has the frequency ω, then two main processes, as noted above, can take place. One of them is third harmonic generation. For this process the tensor $\chi^{(3)}(3\omega; \omega, \omega, \omega, \mathbf{r})$ is responsible. In the medium the waves with frequencies ω and 3ω propagate. These waves have different refractive indices and the wavevectors have different modules with the difference $\Delta k = 3k(\omega) - k(3\omega)$. As already shown (Balyan, 2015*b*), due to this phase mismatch the intensity of the third-harmonic is small and can be neglected. The second essential effect is connected to the tensor $\chi^{(3)}(\omega; \omega, \omega, -\omega, \mathbf{r})$. In this case the incident wave with frequency ω propagates and diffracts in a medium with a self-induced susceptibility. If the wavevector of the incident wave with a certain set of lattice planes forms an angle close to the Bragg angle, then transmitted and diffracted waves will be formed in the crystal. These waves will diffract and propagate in the crystal interacting with each other. This will be the nonlinear dynamical diffraction phenomenon in the crystal. This phenomenon, *i.e.* the third-order nonlinear dynamical diffraction of hard X-rays in crystals, has been considered by Balyan (2015*a*,*b*, 2016*a*,*b*,*c*). An exact solution in a non-absorbing crystal and for the exact Bragg angle was obtained for the symmetrical Laue case by Balyan (2016*b*), and for the symmetrical Bragg case by Balyan (2015*b*).

Under two-wave dynamical diffraction conditions, in the nonlinear case, we have two external free parameters: the deviation from the Bragg exact angle, as in the linear case, and the incident beam intensity. In the present work, continuing the themes of the works of Balyan (2015*a*,*b*, 2016*a*,*b*,*c*), an exact solution is obtained for the third-order nonlinear symmetrical Laue case dynamical diffraction in crystals, which takes into account both the intensity of the incident wave and the deviation from the Bragg exact angle. Using this exact solution, the third-order nonlinear two-wave X-ray dynamical diffraction is investigated. These investigations can be a basis for experimental investigations of the third-order nonlinear dynamical diffraction in crystals, can be used for manufacturing Bragg diffractive optical elements (focusing elements, monochromators and collimators) for high-intensity X-ray beams. The exact solutions have a definite advantage with respect to numerical solutions, since they allow determining the behaviors of essential physical quantities depending on the input parameters. Such essential physical quantities of Bragg diffraction are reflection and transmission coefficients, extinction length, rocking curve full width at half-maximum, the behavior of the wavefields depending on depth and other quantities. The exact solutions also allow finding new effects and new peculiarities of the phenomena under investigation.

2. Theory

In Fig. 1 the scheme of X-ray two-wave symmetrical Laue case dynamical diffraction in a crystal is shown. Under the conditions of X-ray two-wave dynamical diffraction, there are two strong waves inside a crystal: transmitted and diffracted (Authier, 2001; Pinsker, 1982). The electrical field in the crystal,

$$\mathbf{E}(\mathbf{r}) = \mathbf{E}_0(\mathbf{r}) \exp(i\mathbf{K}_0\mathbf{r}) + \mathbf{E}_h(\mathbf{r}) \exp(i\mathbf{K}_h\mathbf{r}), \qquad (1)$$

where $\mathbf{E}_{0,h}$ and $\mathbf{K}_{0,h}$ are the amplitudes and wavevectors of the transmitted and diffracted wave, respectively, $\mathbf{h}$ is the diffraction vector and $\mathbf{K}_h = \mathbf{K}_0 + \mathbf{h}$. The wavevectors are chosen so as to satisfy the Bragg exact condition $\mathbf{K}_h^2 = \mathbf{K}_0^2 = k^2 = (2\pi/\lambda)^2$, where λ is the wavelength. In the third-order nonlinear case the polarization is the sum of the linear polarization and third-order nonlinear polarization (Balyan, 2015*a*,*b*),

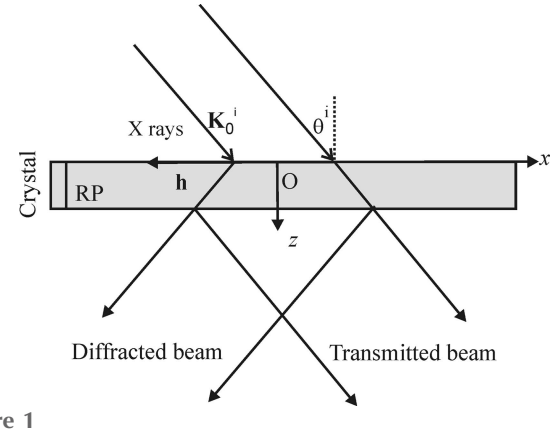

Figure 1
Scheme of X-ray symmetrical two-wave dynamical diffraction, *i.e.* the reflecting lattice planes RP are perpendicular to the entrance surface of the crystal. Shown are $\mathbf{K}_0^i$, the wavevector of the incident beam; θ^i, the angle between the incident wave wavevector and the reflecting planes; $\mathbf{h}$, the diffraction vector; Oxz, the coordinate system in the diffraction plane. Diffracted and transmitted beams emerge from the exit surface.

$$\mathbf{P}(\mathbf{r},\omega)=\mathbf{P}^{(1)}(\mathbf{r},\omega)+\mathbf{P}^{(3)}(\mathbf{r},\omega), \tag{2}$$

where the frequency ω is explicitly shown. The linear polarization is connected to the field through the linear susceptibility (Authier, 2001; Pinsker, 1982),

$$\mathbf{P}^{(1)}(\mathbf{r},\omega)=\varepsilon_0\chi^{(1)}(\mathbf{r},\omega)\,\mathbf{E}(\mathbf{r},\omega). \tag{3}$$

Note that for X-rays $\chi^{(1)}(\omega,\mathbf{r})=-n(\mathbf{r})e^2/(\varepsilon_0 m\omega^2)<0$ and $|\chi^{(1)}(\omega,\mathbf{r})|\simeq 10^{-5}$ to 10^{-6}, where $n(\mathbf{r})$ is the concentration of electrons. The third-order nonlinear polarization in an isotropic medium is connected to the field through the third-order nonlinear susceptibility (Boyd, 2003; Balyan, 2015*a*,*b*),

$$P_i^{(3)}(\mathbf{r},\omega)=3\varepsilon_0\chi_{ijkl}^{(3)}(\omega;\omega,\omega,-\omega,\mathbf{r})\,E_j(\mathbf{r},\omega)\,E_k(\mathbf{r},\omega)\,E_l^*(\mathbf{r},\omega), \tag{4}$$

where i, j, k, l run the values 1, 2 and 3, corresponding to the coordinates x, y and z, and * means the complex conjugate. In (4) the summation over the dummy indices j, k, l is performed. In an isotropic medium, $\chi^{(1)}(\mathbf{r},\omega)$ is a scalar and

$$\chi_{ijkl}^{(3)}(\omega;\omega,\omega,-\omega,\mathbf{r})=\chi_{1122}^{(3)}(\omega;\omega,\omega,-\omega,\mathbf{r})(\delta_{ij}\delta_{kl}+\delta_{ik}\delta_{jl})+\chi_{1221}^{(3)}(\omega;\omega,\omega,-\omega,\mathbf{r})\,\delta_{il}\delta_{jk}, \tag{5}$$

where δ_{ij} is the Kronecker symbol (Boyd, 2003). From (4) and (5),

$$\mathbf{P}^{(3)}=\varepsilon_0 A\mathbf{E}(\mathbf{E}\mathbf{E}^*)+\varepsilon_0 B\mathbf{E}^*(\mathbf{E}\mathbf{E}), \tag{6}$$

where $A=3\chi_{1122}^{(3)}+3\chi_{1221}^{(3)}$, $B=3\chi_{1221}^{(3)}$. For the non-resonant electronic response case [see formula (4.2.13b) of Boyd (2003)], $\chi_{1122}^{(3)}=\chi_{1221}^{(3)}$ and so $B=A/2$. In this case, from (5),

$$\chi_{ijkl}^{(3)}(\omega;\omega,\omega,-\omega,\mathbf{r})=\chi^{(3)}(\omega,\mathbf{r})\,\frac{(\delta_{ij}\delta_{kl}+\delta_{ik}\delta_{jl}+\delta_{il}\delta_{jk})}{3}, \tag{7}$$

where $\chi^{(3)}(\omega,\mathbf{r})=3\chi_{1122}^{(3)}=3\chi_{1221}^{(3)}=\chi_{1111}^{(3)}$. In the work of Balyan (2015*a*) for $\chi^{(3)}(\omega,\mathbf{r})$ the following approximate expression is obtained,

$$\chi^{(3)}\simeq\frac{n(\mathbf{r})\,e^4a_0^4}{\varepsilon_0\hbar^3\omega^3}, \tag{8}$$

where $a_0=5.3\times10^{-11}$ m is the Bohr radius and ω is larger than the resonance frequencies of the electrons in the atoms (non-resonant case). It is convenient to introduce $\eta=A+B$. Using the approximation (7) we have $\eta=3\chi^{(3)}$. Using the values $n(\mathbf{r})\simeq10^{28}$–$10^{30}$ m^{-3} and $\omega=10^{19}$ s^{-1}, from (8) the following estimate $\chi^{(3)}(\omega,\mathbf{r})\simeq10^{-31}$–$10^{-33}$ m^2 V^{-2} is obtained. In a perfect crystal, $n(\mathbf{r})$ is a periodic function of coordinates and therefore $\chi^{(1)}(\mathbf{r},\omega)$ and $\chi^{(3)}(\omega,\mathbf{r})$ (as well as A, B and η) are also periodic functions of coordinates and can be expanded into Fourier series with respect to the reciprocal lattice vectors of the crystal. By this method, as in the linear theory (Takagi, 1969), in the work of Balyan (2015*a*) the third-order nonlinear two-wave dynamical diffraction equations are obtained. We shall consider the case of a σ-polarized plane incident wave (the electric field is perpendicular to the diffraction plane Oxz), the Laue symmetrical case of diffraction (the reflecting lattice planes are perpendicular to the entrance surface of the crystal). The strength of the electrical field [see (1)], in the case of an incident plane wave, can be presented as (Balyan, 2016*b*)

$$E(\mathbf{r})=\exp\left[ik\chi_0 z/(2\cos\theta)\right]\exp(ipx)\times\left[F_0(z)\exp(i\mathbf{K}_0\mathbf{r})+F_h(z)\exp(i\mathbf{K}_h\mathbf{r})\right],$$

where χ_0 is the zero-order Fourier coefficient of $\chi^{(1)}(\mathbf{r})$, $p=k\cos\theta\,\Delta\theta$, $\Delta\theta=\theta^{\rm i}-\theta$ is the deviation of the incident beam from the Bragg exact orientation, $\theta^{\rm i}$ is the angle between the incident wave wavevector and the reflecting lattice planes (Fig. 1) and θ is the Bragg exact angle. The amplitudes satisfy the propagation equations (Balyan, 2016*b*),

$$\begin{aligned}&2ik\cos\theta\frac{{\rm d}F_0}{{\rm d}z}-2kp\sin\theta F_0\\&+k^2\left[\eta_0(|F_0|^2+|F_h|^2)+\eta_h F_0F_h^*+\eta_{\bar h}F_0^*F_h\right]F_0\exp\left(-\frac{\mu z}{\cos\theta}\right)\\&+\left\{k^2\chi_{\bar h}F_h+k^2F_h\exp\left(-\frac{\mu z}{\cos\theta}\right)\right.\\&\left.\times\left[(\eta_0F_0F_h^*+\eta_{\bar h}(|F_0|^2+|F_h|^2)+\eta_{2\bar h}F_0^*F_h)\right]\right\}=0,\end{aligned} \tag{9}$$

$$\begin{aligned}&2ik\cos\theta\frac{{\rm d}F_h}{{\rm d}z}+2kp\sin\theta F_h\\&+k^2\left[\eta_0(|F_0|^2+|F_h|^2)+\eta_h F_0F_h^*+\eta_{\bar h}F_0^*F_h\right]F_h\exp\left(-\frac{\mu z}{\cos\theta}\right)\\&+\left\{k^2\chi_hF_0+k^2F_0\exp\left(-\frac{\mu z}{\cos\theta}\right)\right.\\&\left.\times\left[(\eta_0F_0^*F_h+\eta_h(|F_0|^2+|F_h|^2)+\eta_{2h}F_0F_h^*)\right]\right\}=0.\end{aligned}$$

The following notations are used: $\chi_{0,h,\bar h}$ and $\eta_{0,h,\bar h,2h,2\bar h}$ are the Fourier coefficients for the diffraction vectors $\mathbf{h}$, $\bar{\mathbf{h}}$, $2\mathbf{h}$ and $2\bar{\mathbf{h}}$; $\mu=k\chi_{0\rm i}$ is the linear absorption coefficient, where $\chi_{0\rm i}$ is the zero-order Fourier coefficient of the imaginary part of the linear susceptibility. The boundary conditions are (Balyan, 2016*b*)

$$F_0(0)=E_0^i,\qquad F_h(0)=0. \tag{10}$$

In a non-absorbing crystal (weak absorption) one can put $\mu=0$. Two integrals of motion of the system (9) can be found in non-absorbing crystals (Balyan, 2015*a*, 2016*b*),

$$\begin{aligned}&|F_0(z)|^2+|F_h(z)|^2=\text{const}=|E_0^i|^2=I,\\&p\sin\theta\frac{|F_h|^2-|F_0|^2}{k}+\text{Re}[\chi_hF_0F_h^*]+\frac{\eta_0}{2}|F_0|^2|F_h|^2\\&+\text{Re}[\eta_hIF_0F_h^*]+\frac{1}{2}\text{Re}[\eta_{2h}F_0^2F_h^{*2}]=\text{const}=-\frac{Ip\sin\theta}{k},\end{aligned} \tag{11}$$

where I is the intensity of the incident wave. We formally use the definition 'intensity' for $|E_0^i|^2$, since it is proportional to the modulus of the time-averaged Pointing vector $|\mathbf{S}^i|=0.5c\varepsilon_0|E_0^i|^2$. The first integral of motion is connected to the conservation of the energy flux. Now we have two independent input parameters: $\Delta\theta$ and I. Note that in the linear theory only $\Delta\theta$ defines the behavior of the field inside the crystal. Note also that for obtaining the values of the integrals of motion (11), the boundary conditions (10) are used. It should be mentioned that in a non-absorbing crystal $\chi_{\bar h}=\chi_h^*$ and $\eta_{\bar h,2\bar h}=\eta_{h,2h}^*$. These relations were also used to obtain the integrals of motion.

3. Exact solution

Our purpose is to find the exact solution of the system (9) using the boundary conditions (10) and the integrals of motion (11). The exact solution has been found by Balyan (2016*b*) for the case $p = 0$ (exact Bragg orientation, *i.e.* $\Delta\theta = 0$) and for a forbidden $2\mathbf{h}$ reflection, when $\chi_{2h,2\bar{h}} = 0$, $\eta_{2h,2\bar{h}} = 0$. The symmetrical Laue case has been considered. The solution was presented via Jacobi elliptic functions. Now we will show that the exact solution in a non-absorbing crystal ($\mu = 0$) for the Laue symmetrical case and for the forbidden $2\mathbf{h}$ reflection can also be found for the case $\Delta\theta \neq 0$. Such a solution will depend on the deviation from the exact Bragg angle and the intensity of the incident wave as well. We take $\mu = 0$ and $\eta_{2h,2\bar{h}} = 0$ in (9). Let us present the solution of (9) in the form

$$F_{0,h}(z) = \rho_{0,h}(z)\exp\big[i\varphi_{0,h}(z)\big], \tag{12}$$

where $\rho_{0,h}(z)$ and $\varphi_{0,h}(z)$ are real functions. Note that in the non-resonant electronic response case $\chi^{(1)}(\mathbf{r})$ and $\chi^{(3)}(\mathbf{r})$ have opposite signs and thus the phases of their Fourier coefficients are shifted by π. We can write $\chi_h = |\chi_h|\exp(i\delta)$ and $\eta_h = |\eta_h|\exp(i\delta^{(3)})$, where $\delta^{(3)} = \delta + \pi$. Inserting (12) into (9) and separating the imaginary and real parts, we arrive at the propagation equations for $\rho_{0,h}$ and $\varphi_{0,h}$,

$$\begin{aligned}
&2k\cos\theta\,\dot{\rho}_0 - k^2\chi_{he}\rho_h\sin(\gamma+\delta) = 0,\\
&2k\cos\theta\,\dot{\rho}_h + k^2\chi_{he}\rho_0\sin(\gamma+\delta) = 0,\\
&2k\cos\theta\,\rho_0\dot{\varphi}_0 + \big\{2kp\sin\theta - k^2[\eta_0 I - 2|\eta_h|\rho_0\rho_h\cos(\gamma+\delta)]\big\}\rho_0\\
&\quad - k^2[\eta_0\rho_0\rho_h + \chi_{he}\cos(\gamma+\delta)]\rho_h = 0,\\
&2k\cos\theta\rho_h\dot{\varphi}_h - \big\{2kp\sin\theta + k^2[\eta_0 I - 2|\eta_h|\rho_0\rho_h\cos(\gamma+\delta)]\big\}\rho_h\\
&\quad - k^2[\eta_0\rho_0\rho_h + \chi_{he}\cos(\gamma+\delta)]\rho_0 = 0.
\end{aligned} \tag{13}$$

Here for an arbitrary function $\dot{f} \equiv \mathrm{d}f/\mathrm{d}z$; $\gamma = \varphi_0 - \varphi_h$ and $\chi_{he} \equiv |\chi_h| - |\eta_h|I$ is the effective susceptibility depending on the intensity of the incident wave. As can be seen, in the equations of $\rho_{0,h}$ the difference between the linear and nonlinear theories is the replacement $|\chi_h| \rightarrow \chi_{he}$. For the equations of phases, in the nonlinear case, the deviation parameter p is replaced,

$$p \rightarrow p - k\big[\eta_0 I - 2|\eta_h|\rho_0\rho_h\cos(\gamma+\delta)\big]/(2\sin\theta)$$

for the transmitted beam and

$$p \rightarrow -\big\{p + k\big[\eta_0 I - 2|\eta_h|\rho_0\rho_h\cos(\gamma+\delta)\big]/(2\sin\theta)\big\}$$

for the diffracted beam. These replacements are non-symmetrical with respect to the diffracted and transmitted beam. Therefore an asymmetry will be seen also in the solutions with respect to the sign of p. Note also that in the equations for phases, in the nonlinear case, $|\chi_h| \rightarrow \eta_0\rho_0\rho_h + \chi_{he}\cos(\gamma+\delta)$. Thus in the nonlinear case the beams propagate in a medium with a local deviation parameter and local susceptibilities, which depend on the amplitudes and phases of the waves.

The integrals of motion (11) can be rewritten in a more convenient form,

$$\begin{aligned}
&\rho_0^2 + \rho_h^2 = I,\\
&p\sin\theta\,(\rho_h^2 - \rho_0^2) + \frac{k\eta_0}{2}\rho_0^2\rho_h^2 + k\chi_{he}\rho_0\rho_h\cos(\gamma+\delta) = -Ip\sin\theta.
\end{aligned} \tag{14}$$

The physical meaning of the first integral of motion is the conservation of the energy flux in a non-absorbing crystal. To understand the physical meaning of the second integral of motion let us insert the representation of p via $\Delta\theta$ into (14). Using the first integral of motion in (14), after brief calculations one finds

$$-\frac{\eta_0}{2}\rho_0^2 - \frac{\chi_{he}\rho_0\cos(\gamma+\delta)}{\rho_h} = \alpha, \tag{14a}$$

where $\alpha = \sin 2\theta\Delta\theta$ is the well known deviation parameter from the Bragg exact orientation. This parameter is proportional to the difference of the incident wave wavevector tangential component from the wavevector tangential component corresponding to the exact Bragg orientation. Thus the second integral of motion is connected to the conservation of the tangential component of the incident wave wavevector. Note that for the linear case the equivalent of (14*a*) is $-|\chi_{hr}|\rho_0\cos(\gamma+\delta)/\rho_h = \alpha$. From the second integral of motion, according to (14*a*), one finds immediately that when $\alpha = 0$ the minimal intensity of the transmitted wave can be zero and accordingly the maximal intensity of the diffracted wave can be 1. But when $\alpha \neq 0$ the minimal value of the transmitted wave cannot be zero and accordingly the maximal value of the diffracted wave cannot be 1. This is true also for the linear case.

From (14) one finds

$$\sin(\gamma+\delta) = \pm\frac{1}{\chi_{he}\rho_0}\left[\chi_{he}^2\rho_0^2 - \rho_h^2\left(\frac{2\sin\theta\,p}{k} + \frac{\eta_0}{2}u_0\right)^2\right]^{1/2}. \tag{15}$$

Inserting $\sin(\gamma+\delta)$ into the first equation (13) we have

$$\cos\theta\,\dot{u}_0 \mp k\left\{(I-u_0)\left[\chi_{he}^2 u_0 - (I-u_0)\left(\frac{2\sin\theta\,p}{k} + \frac{\eta_0}{2}u_0\right)^2\right]\right\}^{1/2} = 0 \tag{16}$$

where $u_0 = \rho_0^2$. Here the first integral of motion is used. According to the boundary conditions (10), $u_0(0) = I$. According to the first integral of motion, near the entrance surface, by increasing z, u_0 must decrease and therefore near the entrance surface $\dot{u}_0 < 0$. This means that the '+' sign must be taken in (16) and we have

$$\dot{u}_0 + \frac{2\pi}{\Lambda_e}\left\{(I-u_0)\big[u_0 - (I-u_0)(y+\beta u_0)^2\big]\right\}^{1/2} = 0. \tag{17}$$

Here we used the expression $p = k\cos\theta\,\Delta\theta$ for p and made the notations $\Lambda_e = \lambda\cos\theta/\chi_{he}$, $y = \Delta\theta\sin 2\theta/\chi_{he}$ and $\beta = \eta_0/(2\chi_{he})$. Taking into account $u_0(0) = I$, from (17), we obtain

$$\int\limits_{u_0(z)}^{I} \frac{\mathrm{d}t}{\left\{(I-t)\left[t-(I-t)(y+\beta t)^2\right]\right\}^{1/2}} = \frac{2\pi z}{\Lambda_e}. \qquad (18)$$

The nonlinear theory is based on the perturbation theory. Therefore we must have $|\eta_h I| < |\chi_h|$ and the maximal value of the intensity can be obtained from the equality $|\eta_h| I_{\max} = |\chi_h|$. The variation range of I lies in the range $(0, I_{\max})$, where for the non-resonant electronic response case

$$I_{\max} = |\chi_h|/|\eta_h| = |\chi_0|/|\eta_0| = \frac{\hbar^3\omega}{3me^2a_0^4}. \qquad (19)$$

For estimates we used the expressions for $\chi^{(1)}(\omega, \mathbf{r})$ and for $\chi^{(3)}(\omega, \mathbf{r})$ [formula (8)]. For hard X-rays $I_{\max} \simeq 2.1 \times 10^{25}\ \mathrm{V^2\ m^{-2}}$ and $E_{\max} = (I_{\max})^{1/2} \simeq 4.6 \times 10^{12}\ \mathrm{V\ m^{-1}}$. The modulus of the time-averaged Pointing vector, corresponding to the value $I_{\max} \simeq 2.11 \times 0^{25}\ \mathrm{V^2\ m^{-2}}$, is equal to $|\mathbf{S}^i| = 0.5\, c\, \varepsilon_0\, I_{\max} = 2.8 \times 10^{22}\ \mathrm{W\ m^{-2}} = 2.8 \times 10^{18}\ \mathrm{W\ cm^{-2}}$. Let us briefly consider the experimental capabilities for experiments of plane-wave nonlinear dynamical diffraction effects. If we take a beam of size 50 µm in the diffraction plane, and of size 10 nm (due to the focusing) perpendicular to the diffraction plane direction, the corresponding incident-wave peak power $P = |S^i|\sigma_0 \simeq 14$ GW, where σ_0 is the cross-sectional area of the incident beam. This value can be achieved using synchrotron sources or X-ray free-electron lasers (XFELs). But this is the value for the maximal intensity. Meanwhile the third-order dynamical diffraction effects can be observed also for $0.01 I_{\max} < I \leq 0.1 I_{\max}$ (the nonlinear influence can be accumulated). So, the monochromatization of the beam, which can lead to some loss of intensity, is not crucial and can be achieved. Also the size of the beam perpendicular to the diffraction plane direction can be taken up to 1000 nm. Taking also into account that XFELs can achieve up to 100 GW peak power, instead of 100 nm a beam size of 10^4 nm = 10 µm beam size in the transverse direction can be achieved. Thus experiments of plane-wave nonlinear dynamical diffraction can be performed nowadays.

Passing to the variable $t' = t/I_{\max}$ in (18), one obtains

$$\int\limits_{v_0(z)}^{I_1} \frac{\mathrm{d}t'}{\left\{(I_1-t')\left[t'-(I_1-t')(y+\beta_1 t')^2\right]\right\}^{1/2}} = \frac{2\pi z}{\Lambda_e}, \qquad (20)$$

where $I_1 = I/I_{\max}$, $\beta_1 = \beta I_{\max} = \eta_0 I_{\max}/[2|\chi_h|(1-I_1)] = |\chi_0|/[2|\chi_h|(1-I_1)]$ and $v_0(z) = u_0(z)/I_{\max}$. Formula (20) can be rewritten in the form

$$\int\limits_{v_0(z)}^{I_1} \frac{\mathrm{d}t'}{\left[(I_1-t')(t'-t_1)(t'-t_2)(t'-t_3)\right]^{1/2}} = \frac{2\pi z\beta_1}{\Lambda_e}, \qquad (21)$$

where $t_{1,2,3}$ are the roots of the third-order polynomial under the sign of the square root in (20). The roots of the polynomial have been found in Appendix *A*1.

4. Three cases of exact solution

Let us consider the solutions corresponding to the three cases $Q > 0$, $Q < 0$, $Q = 0$ (see Appendix *A*1). The input parameters $y_0 = \Delta\theta \sin 2\theta/|\chi_h|$ and I_1 define the sign and the value of Q. The parameter y_0 varies in the range $(-\infty, \infty)$ and the parameter I_1 varies in the range $0 < I_1 < 1$. The details of finding the solutions have been given in Appendix *A*2.

Case 1. $Q > 0$. Using (35), after some calculations, for the solution, from equation (21), one finds

$$v_0(z) = \frac{I_1 B_1\left[1+\mathrm{cn}\left(\frac{2\pi z\beta_1}{g\Lambda_e}, \phi\right)\right] + A_1 t_1\left[1-\mathrm{cn}\left(\frac{2\pi z\beta_1}{g\Lambda_e}, \phi\right)\right]}{B_1\left[1+\mathrm{cn}\left(\frac{2\pi z\beta_1}{g\Lambda_e}, \phi\right)\right] + A_1\left[1-\mathrm{cn}\left(\frac{2\pi z\beta_1}{g\Lambda_e}, \phi\right)\right]},$$
$$v_h(z) = \frac{(I_1-t_1)A_1\left[1-\mathrm{cn}\left(\frac{2\pi z\beta_1}{g\Lambda_e}, \phi\right)\right]}{B_1\left[1+\mathrm{cn}\left(\frac{2\pi z\beta_1}{g\Lambda_e}, \phi\right)\right] + A_1\left[1-\mathrm{cn}\left(\frac{2\pi z\beta_1}{g\Lambda_e}, \phi\right)\right]} \qquad (22)$$

where cn is the Jacobi cosine elliptic function. The Jacobi functions are periodic functions of the first argument. Therefore the intensities are periodic functions of the depth and the nonlinear Pendellösung effect takes place, *i.e.* as in the linear theory, the transmitted and diffracted fields periodically interchange by their energies. We will call the Pendellösung distance (period of oscillations) in this case the nonlinear Pendellösung distance Λ_{NL}. According to (35), the expression for this quantity is

$$2\int\limits_{t_1}^{I_1} \frac{\mathrm{d}t'}{\left[(I_1-t')(t'-t_1)(t'-t_2)(t'-t_3)\right]^{1/2}} = \frac{2\pi\Lambda_{\mathrm{NL}}\beta_1}{\Lambda_e}. \qquad (23)$$

The value of the integral of (23) is equal to $gF(\pi, \phi) = 2gK(\phi)$ (Byrd & Friedman, 1971), where $K(\phi)$ is the complete elliptic integral of the first kind. Using this value, from (23),

$$\Lambda_{\mathrm{NL}} = \frac{2g\Lambda_e K(\phi)}{\pi\beta_1}. \qquad (24)$$

Case 2. $Q < 0$. Using the formulas (21) and (36) the solution can be presented as

$$v_0(z) = \frac{I_1(t_1-t_3) + t_3(I_1-t_1)\,\mathrm{sn}^2\left(\frac{2\pi z\beta_1}{g\Lambda_e}, \phi\right)}{t_1-t_3+(I_1-t_1)\,\mathrm{sn}^2\left(\frac{2\pi z\beta_1}{g\Lambda_e}, \phi\right)},$$
$$v_h(z) = \frac{(I_1-t_1)(I_1-t_3)\,\mathrm{sn}^2\left(\frac{2\pi z\beta_1}{g\Lambda_e}, \phi\right)}{t_1-t_3+(I_1-t_1)\,\mathrm{sn}^2\left(\frac{2\pi z\beta_1}{g\Lambda_e}, \phi\right)}. \qquad (25)$$

where sn is the sine Jacobi elliptic function. The behavior of the waves is periodic and the period, *i.e.* the nonlinear Pendellösung distance, according to (36), is defined from the relation

$$2\int_{t_1}^{I_1}\frac{\mathrm{d}t'}{\left[(I_1-t')(t'-t_1)(t'-t_2)(t'-t_3)\right]^{1/2}}=2gF\left(\frac{\pi}{2},\phi\right)=2gK(\phi)=\frac{2\pi\Lambda_{\rm NL}\beta_1}{\Lambda_e}. \quad (26)$$

In (26) we use the fact that in this case $\psi=\pi/2$ and according to the definition $F(\pi/2,\phi)=K(\phi)$. Finally,

$$\Lambda_{\rm NL}=\frac{g\Lambda_e K(\phi)}{\pi\beta_1}. \quad (27)$$

Case 3. $Q=0, q_1<0$. According to Appendix *A*2 the solution is given as

$$v_0(z)=\frac{I_1(t_1-t_3)+t_3(I_1-t_1)\sin^2\left(\frac{2\pi z\beta_1}{g\Lambda_e}\right)}{t_1-t_3+(I_1-t_1)\sin^2\left(\frac{2\pi z\beta_1}{g\Lambda_e}\right)},$$
$$v_h(z)=\frac{(I_1-t_1)(I_1-t_3)\sin^2\left(\frac{2\pi z\beta_1}{g\Lambda_e}\right)}{t_1-t_3+(I_1-t_1)\sin^2\left(\frac{2\pi z\beta_1}{g\Lambda_e}\right)}. \quad (28)$$

Since $K(0)=\pi/2$, for the nonlinear Pendellösung distance from (27) one finds

$$\Lambda_{\rm NL}=g\Lambda_e/(2\beta_1). \quad (29)$$

Consider the case $Q=0, q_1>0$. According to Appendix *A*2 the solution is given as

$$v_0(z)=\frac{I_1(t_1-t_3)+t_3(I_1-t_1)\tanh^2\left(\frac{2\pi z\beta_1}{g\Lambda_e}\right)}{t_1-t_3+(I_1-t_1)\tanh^2\left(\frac{2\pi z\beta_1}{g\Lambda_e}\right)},$$
$$v_h(z)=\frac{(I_1-t_1)(I_1-t_3)\tanh^2\left(\frac{2\pi z\beta_1}{g\Lambda_e}\right)}{t_1-t_3+(I_1-t_1)\tanh^2\left(\frac{2\pi z\beta_1}{g\Lambda_e}\right)}. \quad (30)$$

It is known also that $K(1)=\infty$ (Byrd & Friedman, 1971) and from (27) for the nonlinear Pendellösung distance we have $\Lambda_{\rm NL}=\infty$. In this case the behavior of the field is not periodic. In both last cases (28) and (30) the solution is presented via elementary functions.

The physical meaning of Q can be distinguished passing to the linear case. In this case $I_1\to 0$ and $a\to -y_0$, $c\to -y_0$. It is easy to see that $Q\to(1+y_0^2)^2$. But the jump of the normal component of the incident wave wavevector at the entrance surface is proportional to $(1+y_0^2)^{1/2}$. So Q in the linear case is connected with the jump of the normal component of the wavevector. One can assume that in the non-linear case Q is also a quantity connected with the jump of the normal component of the wavevector. On the other hand Q indicates the region where the Bragg diffraction is not suppressed ($Q>0$) and the region where the Bragg diffraction is abruptly suppressed ($Q<0$). In the last region the energy is mainly concentrated in the transmitted beam. In the nonlinear case, $c=a+I_1\beta_1$ inserting into the expression of Q for Q can be written $Q=(1+a^2)^2/27+a(1+a^2/9)I_1\beta_1/3+I_1^2\beta_1^2/4$. It is interesting that from $a=-y-I_1\beta_1=-(\Delta\theta\sin 2\theta+I\eta_0/2)/\chi_{he}$ it can be seen that a is the deviation parameter corrected by nonlinear refraction. Thus the nonlinear refraction corrects the deviation parameter in the symmetrical case. This enforces our opinion that Q is a parameter connected to the jump of the wavevector on the entrance surface. From the representation of Q it is seen that $Q>0$ for small intensities. It is seen that only the second term in Q can be less than zero. This second term has large values for intensities close to maximal intensity $I_{\rm max}$. For large values of the input intensity $Q\simeq a^4/27+a^3I_1\beta_1/27=-ya^3/27=y(y+I_1\beta_1)^3/27$. If $y>0$, in this region also $Q>0$, but when $y<0$ we have $Q>0$ if $a>0$. Thus when $y<0$ and $a<0$ we have $Q<0$. So in the region where $Q<0$ must be $|y_0|<I_1|\chi_0|/(2|\chi_h|)$, *i.e.* $-I_1|\chi_0|/(2|\chi_h|)<y_0<0$. This allows to localize the region $Q<0$. For Si111, for the $\lambda=0.71$ Å reflection, we have $-0.91<y_0<0$.

5. Discussion and examples

For illustration and discussion of the above obtained results, we will use the Si111 reflection of Mo K_α radiation ($\lambda=0.71$ Å). For this reflection, the reflection Si222 is forbidden, and the obtained exact solution can be used for determination of the wavefield inside the crystal. The behavior of the wavefields is determined by the sign of the parameter $Q(y_0,I_1)=q_1^2/4+q_2^3/27$ (see Appendix *A*1). The sign of this parameter can effectively be determined by its 3D plot. This plot is shown Fig. 2(*a*). For large values of Q the plot is truncated. The regions where $Q(y_0,I_1)$ is positive, negative or zero are clearly seen. We have $Q\le 0$ in the region $I_1>0.5$ and $-1<y_0<0$; $Q>0$ for all y_0 in the region $I_1<0.5$. The sign is also positive for all I_1 in the regions $y_0<-1$ and $y_0>0$. For example the dependence of Q on I_1 for $y_0=-1.1$ and the dependence of Q on y_0 for $I_1=0.1$ are shown in Figs. 2(*b*) and 2(*c*), respectively. In these regions $Q>0$ and the solution is presented by the formula (22). It is convenient to introduce the transmission and reflection coefficients $T=v_0/I_1$, $R=v_h/I_1$. The plots of T and R are shown in Fig. 3. In Fig. 3 the maximal value of μz is equal to 0.1 and therefore the absorption can be neglected. The depth is given in units of $\Lambda_{\rm L}=\Lambda/(1+y_0^2)^{1/2}$, which is the Pendellösung distance in the linear theory for the deviation parameter y_0, and $\Lambda=\lambda\cos\theta/|\chi_h|$ is the extinction distance of the linear theory (Authier, 2001; Pinsker, 1982). For our case, $\Lambda=41.4$ µm and $\Lambda_{\rm L}=27.9$ µm. As can be seen from Fig. 3, the nonlinear Pendellösung distance is greater than $\Lambda_{\rm L}=\Lambda/(1+y_0^2)^{1/2}$. According to (24), $\Lambda_{\rm NL}=29.7$ µm $>\Lambda_{\rm L}$. The behavior of the nonlinear Pendellösung distance, depending on (y_0,I_1), is given by the formulas (27) and (29). The corresponding 3D plot is shown in Fig. 4(*a*). For large values the plot is truncated. As can be seen from Fig. 4(*a*), the nonlinear Pendellösung distance has very large values in the region where $Q\le 0$. In this region the case $Q=0$ can be realized. This corresponds to the situation when the solution is non-periodic [formula (30)]. The dependences $\Lambda_{\rm NL}(-1.1,I_1)$ and $\Lambda_{\rm NL}(y_0,0.1)$ are shown in Figs. 4(*b*) and 4(*c*). For comparison, in the same figures are shown the dependences of the linear Pendellösung distance on I_1 and y_0, respectively.

Let us now consider the solutions in the range $Q\le 0$. According to Fig. 2(*a*) we take $y_0=-0.5$. The dependence

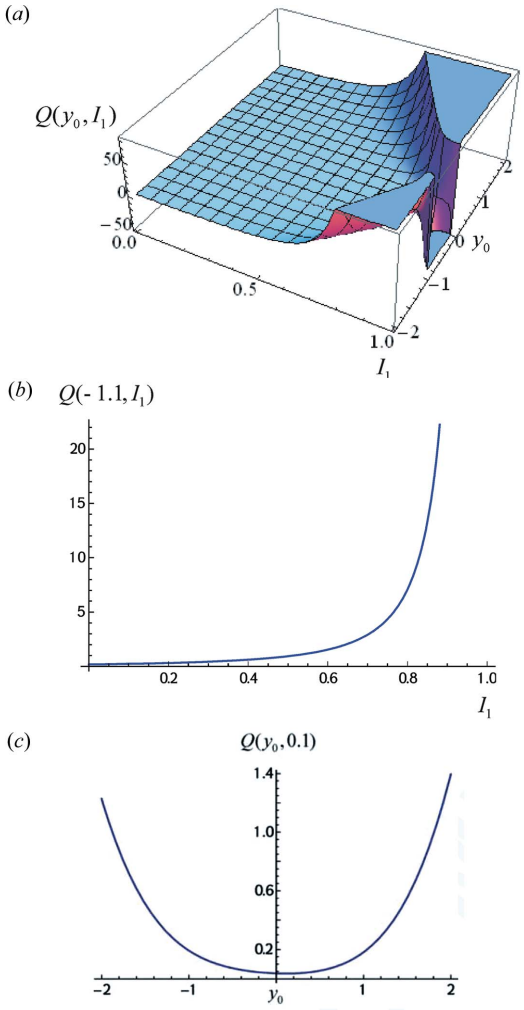

Figure 2
(*a*) 3D plot of the parameter $Q(y_0, I_1)$. Dependences (*b*) $Q(-1.1, I_1)$ and (*c*) $Q(y_0, 0.1)$.

$Q(-0.5, I_1)$ is shown in Fig. 5(*a*). We see that $Q > 0$ in the range $0 < I_1 < 0.908118$, $Q = 0$ at the point $I_1 = 0.908118$ and $Q < 0$ in the range $0.908118 < I_1 < 1$. At the point $I_1 = 0.908118$ we have $q_1 = 2.76 > 0$. Thus, in the range $0 < I_1 < 0.908118$ we have the periodic solutions given by the formula (22). These types of solutions have been shown in Fig. 3. At the point $I_1 = 0.908118$ the solution is given by the formulas (30) and is non-periodic. The solutions at this point are shown in Fig. 5*b*. It should be mentioned that the point $I_1 = 0.908118$ is determined by the precision to six digits and the nonlinear Pendellösung distance at this point is not infinity but is very large, about 1004 µm. At the same time, for $y_0 = -0.5$, the linear Pendellösung distance $\Lambda_L \simeq 37$ µm. The behavior of the nonlinear Pendellösung distance, depending on I_1, on the line $y_0 = -0.5$, is shown in Fig. 5(*c*). It is seen that the Pendellösung distance tends to infinity near the point $I_1 = 0.908118$. The dependence of the nonlinear Pendellösung distance on y_0 for the fixed value $I_1 = 0.908118$ is shown in Fig. 5(*d*). For comparison, the linear case Pendellösung distance is presented as well. In the region $0.908118 < I_1 < 1$ the solutions are given by the formulas (25). The solutions at the point

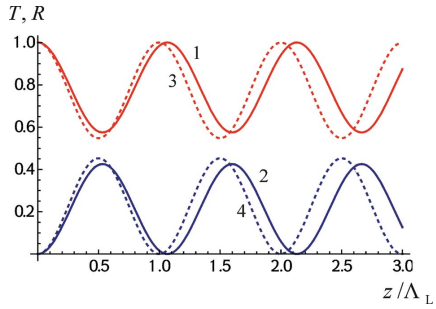

Figure 3
Transmission T and reflection R coefficients in the crystal for the case $Q(-1.1, 0.1) > 0$. Nonlinear case T (solid red curve 1) and R (solid blue curve 2). Linear case T (dotted red curve 3) and R (dotted blue curve 4).

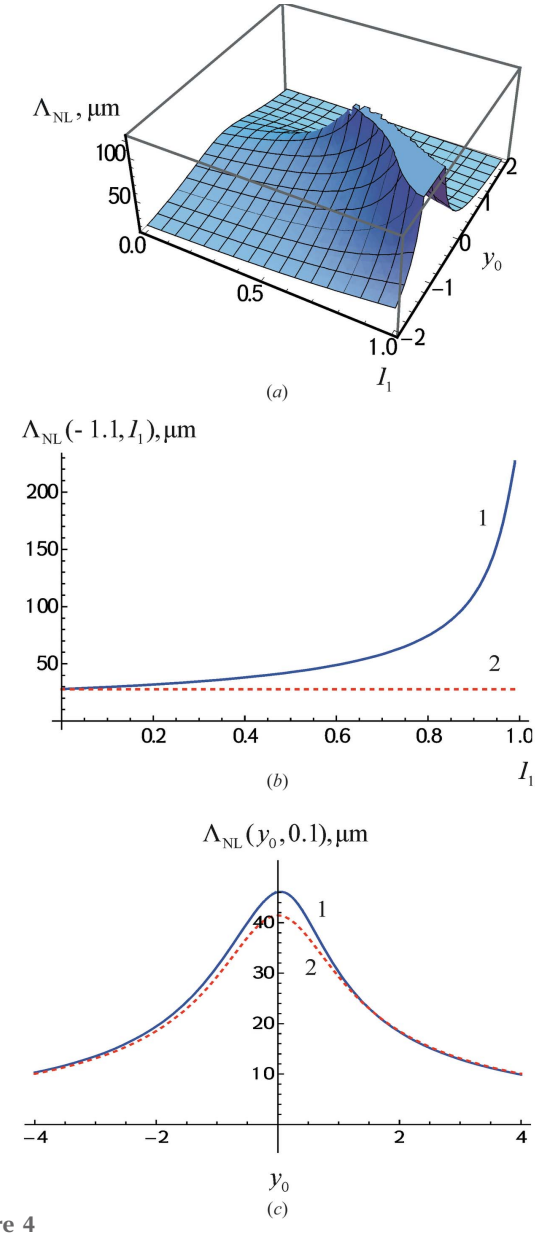

Figure 4
(*a*) 3D plot of the nonlinear Pendellösung distance. (*b*) For fixed value $y_0 = -1.1$, dependences on I_1 of the nonlinear Pendellösung distance (blue solid curve 1) and of the linear Pendellösung distance (red dotted curve 2). (*c*) For fixed value $I_1 = 0.1$, dependences on y_0 of the nonlinear Pendellösung distance (blue solid curve 1) and of the linear Pendellösung distance (red dotted curve 2).

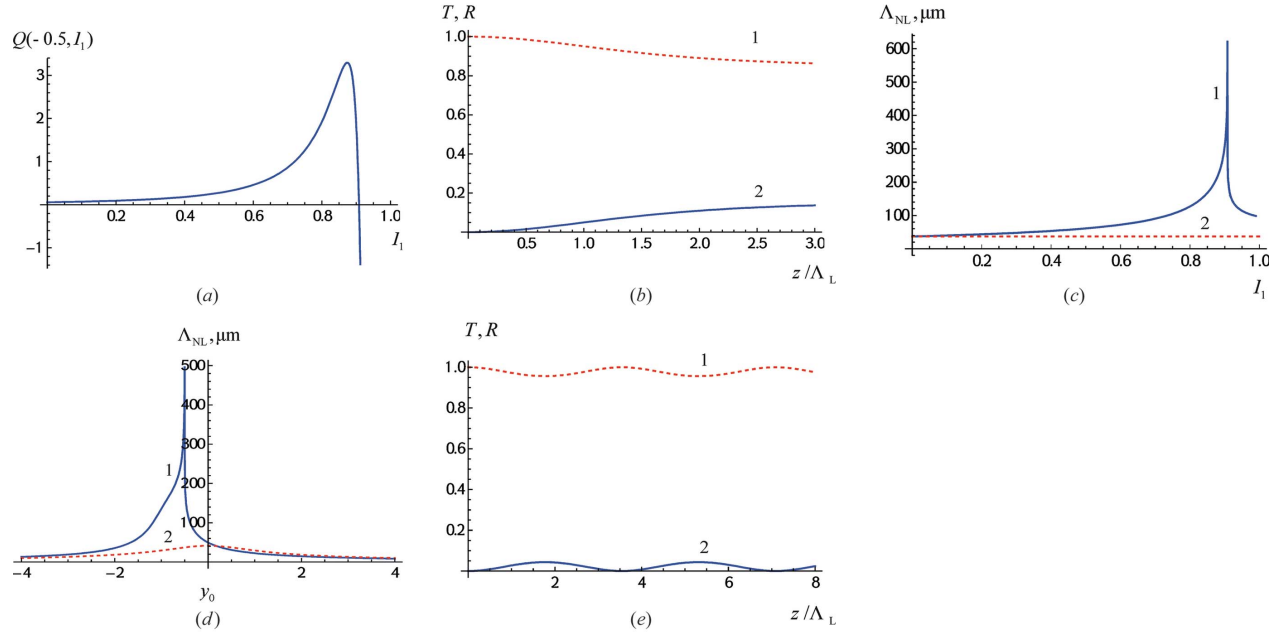

Figure 5
(*a*) The dependence $Q(-0.5, I_1)$. (*b*) T and R of the nonlinear case non-periodic transmitted (red dotted curve 1) and diffracted (blue solid curve 2) waves inside the crystal; $y_0 = -0.5$ and $I_1 = 0.908118$. (*c*) Dependences of the nonlinear Pendellösung distance (blue solid curve 1) and the linear case Pendellösung distance (red dashed curve 2) on I_1 for the fixed value $y_0 = -0.5$. (*d*) Dependences of nonlinear case (blue solid curve 1) and linear case (red dashed curve 2) Pendellösung distances on y_0 for the fixed value $I_1 = 0.908118$. (*e*) The dependences of nonlinear case T and R of transmitted (red dotted curve 1) and diffracted (blue solid curve 2) waves on z for $y_0 = -0.5$ and $I_1 = 0.93$.

$(-0.5, 0.93)$ are shown in Fig. 5(*e*). Note that $\Lambda_{NL} \simeq 131$ μm and $\Lambda_L = 37$ μm.

Now we fix the value of the input intensity, taking $I_1 = 0.7$. The dependence of the parameter $Q(y_0, 0.7)$ is shown in Fig. 6(*a*). The region $-0.1 < y_0 < 0.1$ is shown, to clearly see the behavior near the point $y_0 = 0$. The parameter $Q(y_0, 0.7) > 0$ in the regions $y_0 < -0.0269143$ and $y_0 > 0.0367345$, equals zero at the points $(-0.0269143, 0.7)$ and $(0.0367345, 0.7)$, and is negative in the region $0.0269143 < y_0 < 0.0367345$. It should be noted that $q_1(-0.0269143, 0.7) > 0$ and $q_1(0.0367345, 0.7) < 0$. Thus, according to the theory, in the regions $y_0 < -0.0269143$ and $y_0 > 0.0367345$ we have the periodic solutions (22) (solutions of such types are shown in Fig. 4), at the point $(-0.0269143, 0.7)$ the solutions are non-periodic and are given by the formulas (30) [solutions of such types are presented in Fig. 5(*b*)], at the point $(0.0367345, 0.7)$ the solutions are presented via elementary functions, are periodic and are given by the formulas (28) [see Fig. 6(*b*)], and in the region $-0.0269143 < y_0 < 0.0367345$ the solutions are given by the formulas (25) [see Fig. 6(*c*), where $y_0 = 0.02$]. $\Lambda_{NL} \simeq 79$ μm for the case $(0.0367345, 0.7)$ and $\Lambda_{NL} \simeq 85$ μm for the case $(0.02, 0.7)$. For both cases, $\Lambda_L \simeq 41.4$ μm.

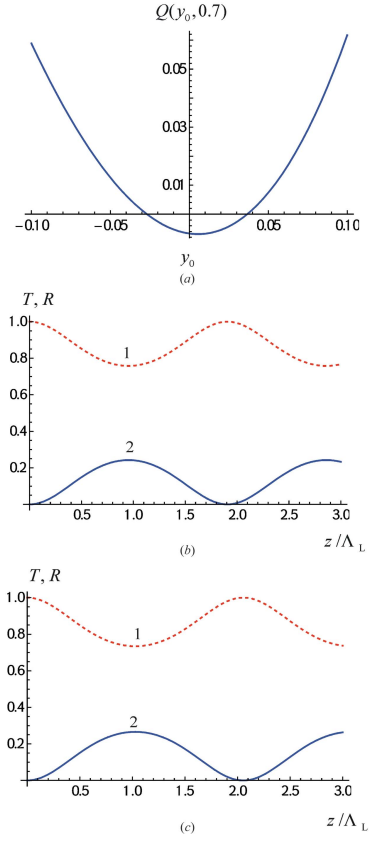

Figure 6
(*a*) Dependence of $Q(y_0, 0.7)$. (*b*) Nonlinear case T (red dotted curve 1) and R (blue solid curve) for $y_0 = 0.0367345$ and $I_1 = 0.7$. (*c*) Nonlinear case T (red dotted curve 1) and R (blue solid curve 2) for $y_0 = 0.02$ and $I_1 = 0.7$.

6. Conclusion

Nonlinear X-ray phenomena became more relevant with the advent of intense X-ray synchrotron sources and XFELs. In this work the third-order nonlinear X-ray two-wave dynamical diffraction in crystals is considered. A new exact solution for

the Laue symmetric case of diffraction is obtained. The exact solution is presented via Jacobi elliptic functions. Two essential input parameters are the deviation parameter from exact Bragg direction and the intensity of the incident wave. The sign of a parameter, being the combination of these two parameters, defines the behavior of the wavefield inside the crystal. The exact solutions of three different types are found, corresponding to the positive and the negative signs of this parameter and to its zero value. For the non-zero values of this combined parameter the solutions are periodic and a nonlinear Pendellösung effect takes place. For the nonlinear Pendellösung distance, the appropriate formulas are obtained. For some zero values of the mentioned parameter the solutions are nonperiodic and are presented via elementary functions. The Pendellösung distance in this case tends to infinity. In comparison with the linear Pendellösung distance, the nonlinear one is greater due to the fact that the third-order nonlinear susceptibility has the opposite sign of the linear one. The obtained exact solution can be a base for experimental investigations of the third-order nonlinear dynamical diffraction, can be used for preparation of intense X-ray beams with given parameters, for manufacturing X-ray Bragg diffractive elements (monochromators, collimators, focusing elements) and for investigation of nonlinear X-ray interaction with matter.

APPENDIX *A*
Finding the roots and solutions

A1. Finding the roots

Let us denote $P_4(t') = (I_1 - t')[t' - (I_1 - t')\,(y + \beta_1 t')^2] = (I_1 - t')\,P_3(t')$. One of the roots of the polynomial $P_4(t')$ is $t_0' = I_1$. To determine the value of the integral (21), we must find the remaining three roots of the polynomial $P_3(t') = t' - (I_1 - t')(y + \beta_1 t')^2$. Note, when $t' < 0$, then $P_3(t') < 0$ and there are no roots. When $t' > I_1$, $P_3(t') > 0$ and there are no roots. Thus, the roots of $P_3(t')$ are in the range $0 \le t' \le I_1$. Since for $t' > I_1$ we have $P_4(t') < 0$, then we must have $t' \le I_1$ inside the crystal. On the other hand, for $t' < 0$ we have $P_4(t') < 0$ and, thus, we must have $t' \ge 0$ inside the crystal. The polynomial $P_3(t') = \beta_1^2(t'^3 + a_1 t'^2 + b_1 t' + c_1) = \beta_1^2(t' - t_1)(t' - t_2)(t' - t_3)$ where $a_1 = 2y/\beta_1 - I_1$, $b_1 = (1 + y^2 - 2y\beta_1 I_1)/\beta_1^2$, $c_1 = -y^2 I_1/\beta_1^2$ and t_1, t_2 and t_3 are the roots of the polynomial $P_3(t')$.

To find the roots of the polynomial $P_3(t') = 0$ it is more convenient to pass to the variable $t'' = y + \beta_1 t'$. The polynomial takes the form $P_3(t'') = (t''^3 + a t''^2 + b t'' + c)/\beta_1$, where $a = -(y + I_1\beta_1)$, $b = 1$, $c = -y$. Thus, if one finds the roots in terms of t'', then using the relation $t' = (t'' - y)/\beta_1$ the roots in terms of t' can be found. As is well known, the roots of the polynomial of the third-order are given by Cardano's formula (Kurosh, 1980; Korn & Korn, 1968). Cardano's formula for our case has the following form,

$$t_i = \frac{\alpha_1 + \alpha_2 - (a/3) - y}{\beta_1}, \quad i = 1, 2, 3, \tag{31}$$

where

$$\alpha_1 = \sqrt[3]{-q_1/2 + \left(q_1^2/4 + q_2^3/27\right)^{1/2}},$$

$$\alpha_2 = \sqrt[3]{-q_1/2 - \left(q_1^2/4 + q_2^3/27\right)^{1/2}},$$

$q_1 = 2a^3/27 - a/3 + c$ and $q_2 = 1 - a^2/3$. Each cubic root α_1 and α_2 has three values. But in (31) such values must be taken for which $\alpha_1\alpha_2 = -q_2/3$. For the polynomial P_3 the coefficients are real. Let us denote $Q = q_1^2/4 + q_2^3/27$. The following cases must be distinguished

1. $Q > 0$. In this case the polynomial has a real root and two complex conjugated roots,

$$\begin{aligned} t_1 &= \frac{\alpha_1 + \alpha_2 - (a/3) - y}{\beta_1}, \\ t_2 &= \left(-\frac{\alpha_1 + \alpha_2}{2} + i\sqrt{3}\,\frac{\alpha_1 - \alpha_2}{2} - a/3 - y\right)/\beta_1, \\ t_3 &= t_2^*, \end{aligned} \tag{32}$$

where we take as α_1 the real value of the cubic root in (31).

2. $Q < 0$. There are three real and not equal roots,

$$\begin{aligned} t_1 &= \left[2(-q_2/3)^{1/2}\cos(\varphi/3) - a/3 - y\right]/\beta_1, \\ t_2 &= \frac{(-q_2/3)^{1/2}\cos(\varphi/3) - (-q_2)^{1/2}\sin(\varphi/3) - a/3 - y}{\beta_1}, \\ t_3 &= \frac{(-q_2/3)^{1/2}\cos(\varphi/3) + (-q_2)^{1/2}\sin(\varphi/3) - a/3 - y}{\beta_1}, \end{aligned} \tag{33}$$

where $\cos\varphi = -q_1/[2(-q_2^3/27)^{1/2}]$ ($q_2 < 0$ in this case). Let us redefine $t_1 = \max(t_1, t_2, t_3)$ and $t_3 = \min(t_1, t_2, t_3)$, *i.e.* in the new notations $t_3 < t_2 < t_1$.

3. $Q = 0$. In this case there are three real roots and two of them are equal,

$$\begin{aligned} t_1 &= \left[2(-q_1/2)^{1/3} - a/3 - y\right]/\beta_1, \\ t_2 &= t_3 = \left[(-q_1/2)^{1/3} - a/3 - y\right]/\beta_1. \end{aligned} \tag{34}$$

Note that we take the real root of $(-q_1/2)^{1/3}$.

A2. Finding the solutions

In the case $Q > 0$ it is known that the integral (Byrd & Friedman, 1971)

$$\begin{aligned} \int_{t_1}^{v_0(z)} \frac{\mathrm{d}t'}{\left[(I_1 - t')(t' - t_1)(t' - t_2)(t' - t_2^*)\right]^{1/2}} &= g\,\mathrm{cn}^{-1}(\cos\psi, \phi) \\ &= gF(\psi, \phi), \end{aligned} \tag{35}$$

$F(\psi, \phi)$ is the normal elliptic integral of the first kind, $g = 1/(A_1B_1)^{1/2}$,

$$\cos\psi = \left\{\left[I_1 - v_0(z)\right]B_1 - \left[v_0(z) - t_1\right]A_1\right\} \Big/ \left\{\left[I_1 - v_0(z)\right]B_1 + \left[v_0(z) - t_1\right]A_1\right\},$$

$$A_1^2 = (I_1 - \mathrm{Re}\,t_2)^2 + (\mathrm{Im}\,t_2)^2,$$

$$B_1^2 = (t_1 - \mathrm{Re}\,t_2)^2 + (\mathrm{Im}\,t_2)^2,$$

$\phi^2 = [(I_1 - t_1)^2 - (A_1 - B_1)^2]/(4A_1B_1)$.

In the case $Q < 0$ it is known that the integral (Byrd & Friedman, 1971)

$$\int_{v_0(z)}^{I_1} \frac{\mathrm{d}t'}{\left[(I_1 - t')(t' - t_1)(t' - t_2)(t' - t_3)\right]^{1/2}} = g\,\mathrm{sn}^{-1}(\sin\psi, \phi) = gF(\psi, \phi), \quad (36)$$

where $g = 2/[(I_1 - t_2)(t_1 - t_3)]^{1/2}$,

$$\sin\psi = \left\{(t_1 - t_3)\left[I_1 - v_0(z)\right]\right\}^{1/2} \Big/ \left\{(I_1 - t_1)\left[v_0(z) - t_3\right]\right\}^{1/2}$$

and $\phi^2 = [(I_1 - t_1)(t_2 - t_3)]/[(I_1 - t_2)(t_1 - t_3)]$.

In the case $Q = 0$, $q_1 < 0$, there are three real roots and two of them are equal [see (34)]. In (34), $t_1 > t_2$ (since $q_1 < 0$) and the solution can be obtained from (25) as the limit when $t_2 = t_3$. For $t_2 = t_3$ we have $\phi = 0$ [see (36)]. It is known that $\mathrm{sn}(u, 0) = \sin u$ (Byrd & Friedman, 1971). Inserting this value into (25), the solution (28) is obtained.

In the case $Q = 0$, $q_1 > 0$, in the formula (25) $t_2 = t_3 > t_1$. Redefining in (25) $t_1 = t_2 = [(-q_1/2)^{1/3} - a/3 - y]/\beta_1$, $t_3 = [2(-q_1/2)^{1/3} - a/3 - y]/\beta_1$, we can obtain the solution from (25) taking $t_1 = t_2$. Now in (25), $\phi = 1$. It is known that $\mathrm{sn}(u, 1) = \tanh u$ (Byrd & Friedman, 1971) and from (25) we find the solution (30).

References

Adams, B., Fernandez, P., Lee, W.-K., Materlik, G., Mills, D. M. & Novikov, D. V. (2000). *J. Synchrotron Rad.* **7**, 81–88.

Adams, B. W. (2003). Editor. *Nonlinear Optics, Quantum Optics, and Ultrafast Phenomena with X-rays: Physics with X-rays Free Electron Lasers.* New York: Springer Science + Business.

Authier, A. (2001). *Dynamical theory of X-ray Diffraction.* Oxford University Press.

Balyan, M. K. (2015*a*). *Crystallogr. Rep.* **60**, 993–1000.

Balyan, M. K. (2015*b*). *J. Synchrotron Rad.* **22**, 1410–1418.

Balyan, M. K. (2016*a*). *J. Contemp. Phys.* **51**, 391–397.

Balyan, M. K. (2016*b*). *Crystallogr. Rep.* **61**, 1039–1046.

Balyan, M. K. (2016*c*). *J. Synchrotron Rad.* **23**, 919–928.

Barbiellini, B., Joly, Y. & Tamasaku, K. (2015). *Phys. Rev. B*, **92**, 155119.

Borodin, D., Levy, S. & Shwartz, S. (2017). *Appl. Phys. Lett.* **110**, 131101.

Borodin, D., Schori, A., Rueff, J.-P., Ablett, J. M. & Shwartz, S. (2019). *Phys. Rev. Lett.* **122**, 023902.

Boyd, R. (2003). *Nonlinear Optics*, 3rd ed. New York: Academic Press.

Bushuev, V. A. & Kuz'min, V. R. (1977). *Sov. Phys. Usp.* **20**, 406–431.

Byrd, P. F. & Friedman, M. D. (1971). *Handbook of Elliptic Integrals for Engineers and Scientists*, 2nd ed., New York: Springer-Verlag.

Cohen, R. & Shwartz, S. (2019). *Phys. Rev. Res.* **1**, 033133.

Conti, C., Fratalocchi, A., Ruocco, G. & Sette, F. (2008). *Opt. Express*, **16**, 8324–8331.

Danino, H. & Freund, I. (1981). *Phys. Rev. Lett.* **46**, 1127–1130.

Doumy, G., Roedig, C., Son, S.-K., Blaga, C. I., DiChiara, A. D., Santra, R., Berrah, N., Bostedt, C., Bozek, J. D., Bucksbaum, P. H., Cryan, J. P., Fang, L., Ghimire, S., Glownia, J. M., Hoener, M., Kanter, E. P., Krässig, B., Kuebel, M., Messerschmidt, M., Paulus, G. G., Reis, D. A., Rohringer, N., Young, L., Agostini, P. & DiMauro, L. F. (2011). *Phys. Rev. Lett.* **106**, 083002.

Eisenberger, P. & McCall, S. L. (1971). *Phys. Rev. Lett.* **26**, 684–688.

Freund, I. (1972). *Chem. Phys. Lett.* **12**, 583–588.

Freund, I. & Levine, B. F. (1969). *Phys. Rev. Lett.* **23**, 854–857.

Freund, I. & Levine, B. F. (1970). *Phys. Rev. Lett.* **25**, 1241–1245.

Fuchs, M., Trigo, M., Chen, J., Ghimire, S., Shwartz, S., Kozina, M., Jiang, M., Henighan, T., Bray, C., Ndabashimiye, G., Bucksbaum, P. H., Feng, Y., Herrmann, S., Carini, G. A., Pines, J., Hart, P., Kenney, Ch., Guillet, S., Boutet, S., Williams, G. J., Messerschmidt, M., Seibert, M. M., Moeller, S., Hastings, J. B. & Reis, D. A. (2015). *Nat. Phys.* **11**, 964–970.

Geloni, G., Saldin, E., Schneidmiller, E. & Yurkov, M. (2007). *Opt. Commun.* **271**, 207–218.

Glover, D. E., Fritz, D. M., Cammarata, M., Allison, T. K., Coh, S., Feldkamp, D. M., Lemke, H., Zhu, D., Feng, Y., Coffee, R. N., Fuchs, M., Ghimire, S., Chen, J., Shwartz, S., Reis, D. A., Harris, S. E. & Hastings, J. B. (2012). *Nature*, **488**, 603–608.

James, R. W. (1950). *The Optical Principles of the Diffraction of X-rays.* London: G. Bell and Sons.

Kolpakov, A. V., Bushuev, V. A. & Kuz'min, R. N. (1978). *Sov. Phys. Usp.* **21**, 959–977.

Korn, G. A. & Korn, T. M. (1968). *Mathematical Handbook for Scientists and Engineers.* New York: McGraw Hill.

Kurosh, A. (1980). *Higher Algebra.* Moscow: Mir Publishers.

Minerbi, E. & Shwartz, S. (2019). *J. Opt. Soc. Am. B*, **36**, 624–630.

Nazarkin, A., Podorov, S., Uschmann, I., Förster, E. & Sauerbrey, R. (2003). *Phys. Rev. A*, **67**, 041804.

Pinsker, Z. G. (1982). *X-ray Crystal Optics.* Moscow: Nauka.

Schori, A., Bömer, C., Borodin, D., Collins, S., Detlefs, B., Moretti Sala, M., Yudovich, S. & Shwartz, S. (2017). *Phys. Rev. Lett.* **119**, 253902.

Shwartz, E. & Shwartz, S. (2015). *Opt. Express*, **23**, 7471–7480.

Shwartz, S., Coffee, R. N., Feldkamp, J. M., Feng, Y., Hastings, J. B., Yin, G. Y. & Harris, S. E. (2012). *Phys. Rev. Lett.* **109**, 013602.

Shwartz, S., Fuchs, M., Hastings, J. B., Inubushi, N., Ishikawa, T., Katayama, T., Reis, D. A., Sato, T., Tono, K., Yabashi, M., Yudovich, S. & Harris, S. E. (2014). *Phys. Rev. Lett.* **112**, 163901.

Takagi, S. (1969). *J. Phys. Soc. Jpn*, **26**, 1239–1253.

Tamasaku, K. & Ishikawa, T. (2007*a*). *Phys. Rev. Lett.* **98**, 244801.

Tamasaku, K. & Ishikawa, T. (2007*b*). *Acta Cryst.* A**63**, 437–438.

Tamasaku, K., Sawada, K. & Ishikawa, T. (2009). *Phys. Rev. Lett.* **103**, 254801.

Tamasaku, K., Shigemasa, E., Inubushi, Y., Katayama, T., Sawada, K., Yumoto, Ohashi, H., Mimura, H., Yabashi, M., Kazuto Yamauchi, K. & Ishikawa, T. (2014). *Nat. Photon. Lett.* **8**, 313–316.

Tanaka, S. & Mukamel, S. (2002). *Phys. Rev. Lett.* **89**, 043001.

Yoda, Y., Suzuki, T., Zhang, X.-W., Hirano, K. & Kikuta, S. (1998). *J. Synchrotron Rad.* **5**, 980–982.

Yudovich, S. & Shwartz, S. (2015). *J. Opt. Soc. Am. B*, **32**, 1894–1900.